IEICE TRANSACTIONS

on Electronics

DOI:10.1587/transele.2023ECP5057

Publicized:2024/05/02

A PUBLICATION OF THE ELECTRONICS SOCIETY

The Institute of Electronics, Information and Communication Engineers
Kikai-Shinko-Kaikan Bldg., 5-8, Shibakoen 3chome, Minato-ku, TOKYO, 105-0011 JAPAN

PAPER

Design of Broadband Resonant Transmission for Depth-focused Waveform in GAFDEM Exploration

Shengbao YU[†], ***Nonmember,*** **Fanze MENG**[†], ***Nonmember***, **Yihan SHEN**[†], ***Nonmember***, **Yuzhu HAO**[†], ***Nonmember, and*** **Haigen ZHOU**[†a)], ***Nonmember***

SUMMARY The Ground-Air Frequency Domain Electromagnetic Method (GAFDEM) is a fast and effective semi-airborne electromagnetic exploration method for subsurface anomaly targets. Based on the depth-focused transmission waveform, this method can realize the high-resolution detection of underground targets at specific depths. However, due to the high inductance and resistance parameters of the transmitting load in GAFDEM exploration, the transmission current of the depth-focused waveform decays rapidly in the middle and high-frequency bands, which restricts the detection signal intensity. To solve this problem, a broadband resonant circuit and its parameter design method are proposed. According to the typical transmission frequency range and load, the parameters are designed, and the circuit model is simulated and tested. The results show that the designed broadband resonant circuit can increase the transmission active power of the depth-focused waveform by more than 490%, reduce the reactive power by more than 37%, and increase the transmission current intensity of the target frequency by 2.64 times. Moreover, this circuit has good robustness. It can achieve a good resonance effect within the error range of ±10% of capacitor. This design provides an effective way for GAFDEM to enhance the intensity of high-frequency detection signals and improve the shallow exploration effect.

key words: *broadband-resonant, depth-focused waveform, electromagnetic transmitter, GAFDEM*

1. Introduction

The Ground-Air Frequency Domain Electromagnetic Method (GAFDEM) is a semi-airborne electromagnetic detection method developed rapidly in recent years. It is mainly used for the rapid exploration of underground structures in complex terrain [1], [2]. This method adopts the working modes of ground transmission and air reception. It takes into account the characteristics of the large detection depth of ground detection methods and the high detection efficiency of airborne electromagnetic methods [3]–[7]. GAFDEM uses grounded conductor sources to emit current waveforms of different frequencies into the ground to detect different depths. Its commonly used operating frequency is 10 Hz–10 kHz, and above 1 kHz is the medium-high frequency band, which is mainly used for detecting shallow targets. GAFDEM initially adopted the square wave as the transmission waveform, which has only one available fundamental frequency with a large amplitude, and its detection efficiency is low [8], [9]. To improve the detection efficiency, GAFDEM further adopted the 2^n pseudo-random sequence as the transmission waveform. This waveform can transmit multiple frequency points at a time, greatly improving detection efficiency [10], [11], but the frequency points of the waveform are relatively dispersed, and the longitudinal resolution is limited. To further improve the resolution, Lihui Gao et al. proposed a depth-focused waveform based on Selective Harmonic Elimination PWM (SHEPWM) in recent years [12], [13]. This waveform exhibits multiple high-order harmonics with significant amplitudes, and the harmonic orders are relatively concentrated. It can transmit multiple densely distributed frequency points and has the characteristics of high longitudinal resolution, which is suitable for detailed and efficient detection of specific target depth. However, GAFDEM uses long wires and grounding electrodes as transmitting loads, which have high inductance and resistance. In the middle and high-frequency bands, the load impedance is high. This makes it difficult for the depth-focused waveform to emit a large current, which limits the detection effect of the shallow part.

Aiming at the problem of the high-frequency impedance of the load, Qihui Zhen and Qingyun Di increased the amplitude of the high-frequency transmission current by changing the topology of the transmitter circuit [14]. This method has a certain effect on current enhancement, but it increases the complexity of the instrument and requires high reliability of the hardware. Meng Wang and Haigen Zhou et al. improved the excitation ability of artificial sources by changing the number of excitation sources [15]–[17]. Although this method can improve the resolution of shallow exploration, it increases the number and complexity of instruments, the cost, and the construction difficulties. Xiujuan Wang, Zhihong Fu et al. used a high-voltage clamp to widen the frequency band, but it is mainly suitable for magnetic sources with small resistance and inductance [18]. Kim, Jungsik et al. and Yongming Zao et al. used resonance to enhance the amplitude of current, which is a simple and effective way [19]–[21]. However, conventional narrow-band resonance is mainly targeted at a single frequency point, so it is not suitable for multi-frequency transmission waveforms. To

†The authors are with the college of Instrumentation and Electrical Engineering of Jilin University, Changchun, 130012, P.R. China

a) E-mail: zhouhaigen@jlu.edu.cn

realize multi-frequency transmission, Changsheng Liu et al. proposed the method of combining the third-order 2^n pseudo-random waveform with three-frequency resonance [22]. On this basis, Shuxu Liu proposed a resonance design method with more frequencies [23]. This method achieves high-frequency, multi-frequency, and large current transmission, but it increases the number of devices in the transmitter system. The solution of circuit parameters is complicated, and the precision of resonance matching is required to be high. Small device parameter deviations will have a great impact on the resonance effect, affecting the field applicability of the method [24], [25].

To solve the above problems, a broadband resonant circuit suitable for the depth-focused waveform was designed in this paper. The key advantage of this circuit lies in its ability to significantly enhance the amplitudes of multiple major harmonics in the deep focus waveform using just a single capacitor. This approach greatly simplifies the complexity of the transmitter system. The proposed circuit design method is of great significance for improving the transmitting capability of the electromagnetic method in the middle and high-frequency bands and increasing the signal intensity. In the following part, we first introduce the GAFDEM, further, describe the depth-focused waveform broadband resonant circuit design process, and finally give the simulation and experimental results. The proposed circuit design method is of great significance for improving the transmission capability of the GAFDEM in the middle and high-frequency bands.

2. Ground-Air Frequency Domain Electromagnetic method

Fig. 1 shows the structure and working mode of the GAFDEM system, which mainly includes the ground transmitter system and the air receiving system. The ground transmitter system is used to radiate electromagnetic energy into space and excite underground anomalous targets. The airborne receiving system is used to collect electromagnetic response signals in space and detect underground anomalous targets. Among them, the ground transmitter system mainly includes a power supply, transmitter, grounding electrode, and transmission wire [26]. The simplified circuit equivalent model of the ground part of the GAFDEM system is shown in Fig. 2. The main functional circuit of the transmitter can be equivalent to the inverter circuit. The transmission wire and grounding electrode can be equivalent to a load of resistance and an inductor in series in the case of single-power supply transmission [27]. The total resistance of the electrode and transmission wire is generally 10–80 Ω [28]. The length of the transmission wire is generally 500 m–5 km [29], and the equivalent inductance L is about 1.1 mH–13.6 mH.

In practice, the transmitter system generates a specific voltage waveform U_o from the inverter and exerts it on the loads to generate a multi-frequency transmission current.

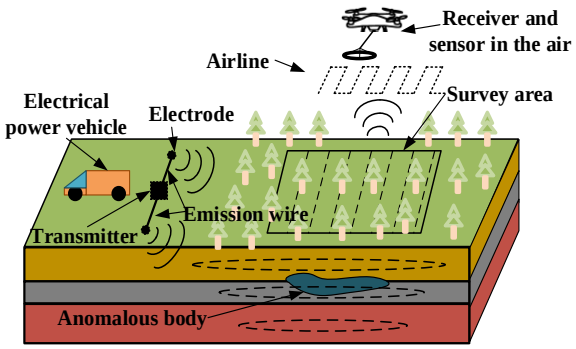

Fig. 1 Schematic diagram of GAFDEM.

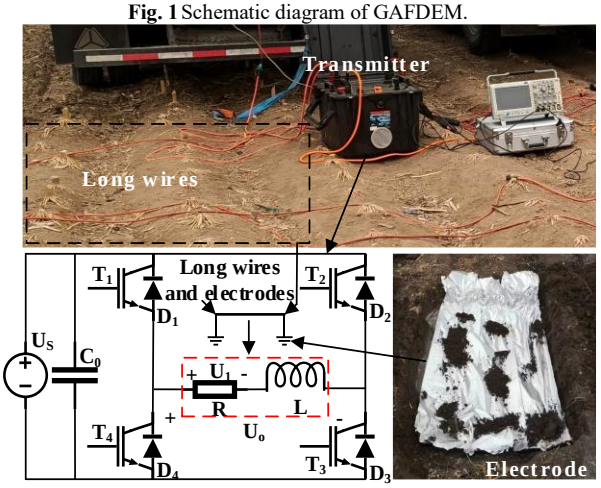

Fig. 2 Schematic diagram of a simplified equivalent model of the transmitter circuit.

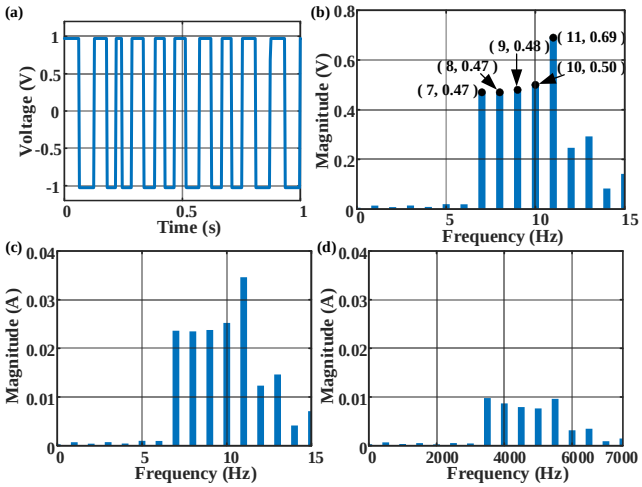

Fig. 3 Waveform of depth-focused waveform and transmission spectrum. (a) Waveform. (b) Energy distribution. (c)Spectrum with 1 Hz fundamental frequency. (d) Spectrum with 500 Hz fundamental frequency.

Fig. 3(a) shows an actual depth-focused waveform, which corresponds to the output voltage U_o of the inverter shown in Fig. 2. The waveform is generated by the following steps: (1) Set the frequency domain information of the output voltage of the inverter according to the desired harmonic order. (2) SHEPWM nonlinear equations are obtained according to the frequency domain information of the power supply. (3) The switching time of the inverter is obtained by solving the nonlinear equations [12], [13]. The waveform is bipolar, with positive and negative transformations. The

actual harmonic frequency can be controlled by adjusting the timing of positive and negative polarity changes. Fig.3(b) shows the wave energy distribution. When the inverter power supply voltage is 1 V, the 7-11 times harmonic magnitudes are 0.47 V, 0.47 V, 0.48 V, 0.50 V, and 0.69 V. If the inverter power supply voltage is known, the voltage magnitude of each harmonic can be obtained based on the energy contribution of each harmonic. Figs. 3(c) and 3(d) show the depth-focused waveform spectrum with fundamental frequencies of 1 Hz and 500 Hz, respectively, under the same circuit parameters. it can be seen that after the fundamental frequency increases to 500 Hz, all harmonics produce significant attenuation with a reduced range of more than 50%. The main reason is that the impedance of the transmission load increases as the frequency increases. In GAFDEM, the attenuation of waveform amplitude will directly reduce the intensity of the detection signal, reduce the detection area, and affect the actual detection effect.

3. Matching mode and parameter design

3.1 Matching mode

To solve the problem of the high impedance of the load, the resonant matching principle was adopted in this paper. Different from the traditional RLC resonance, the proposed broadband resonance method has the following differences: (1) The traditional RLC resonance is only for a frequency at the resonant point, that is, a capacitor is used to match a frequency, while the broadband resonance is used for multiple frequencies in the passband, that is, a capacitor is used to match all the harmonic frequencies of the depth-focused waveform. (2) The traditional RLC selects the matching capacitor according to the required frequency and inductance value, while the broadband resonance determines the pass band according to the harmonic distribution of the depth-focused waveform and then selects the resonant point and the matching capacitor. Fig. 4 shows a schematic diagram of the resonant effect in this paper. It can be seen that the resonant effect in this paper is intended to use a matching capacitor to simultaneously increase multiple harmonic magnitudes, rather than the current amplitude at a specific resonant frequency.

Fig. 5(a) shows the multi-frequency narrowband

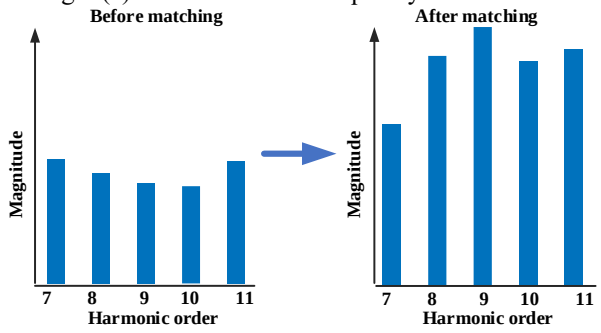

Fig. 4 Schematic diagram of the resonant effect.

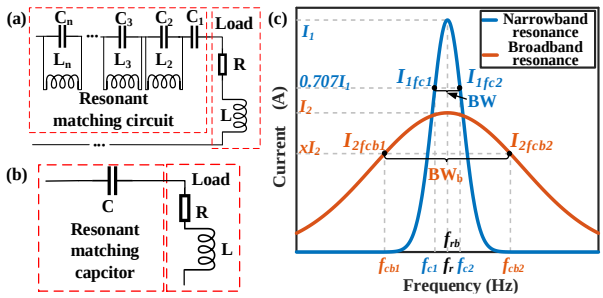

Fig. 5 Comparison of broadband and narrowband resonant circuit diagrams and amplitude-frequency characteristic curves. (a) Narrowband resonant circuit diagram [22], [23]. (b) Broadband resonant circuit diagram. (c) Amplitude-frequency characteristics of the broadband circuit and the multi-frequency narrowband resonance circuit at one frequency point.

resonance method. L and R are equivalent models of transmission wire and grounding electrode, and C_1-C_n and L_2-L_n are resonant matching circuits. This method can be regarded as a combination of multiple traditional RLC resonators. To realize the resonance of multiple depth-focused frequency points, it is necessary to increase the number of resonant capacitors and inductors. This makes the calculation of circuit parameters very complicated. To reduce the difficulty of circuit design, the broadband resonant circuit shown in Fig. 5(b) is adopted in this paper to achieve multi-frequency resonance of the depth-focused waveform. Compared with Fig. 5(a), the circuit shown in Fig. 5(b) has only one capacitor, C. By taking advantage of the characteristics of GAFDEM's large resistance load, a wider passband is obtained, thus realizing the multi-frequency enhancement of the depth-focused waveform. Fig. 5(c) shows the current-frequency curve of a multi-frequency resonance or a conventional RLC resonance and a broadband resonant circuit. Wheref_r, f_{c2}, f_{c1}, BW, I_1, $I_{1f_{c2}}$, $I_{1f_{c1}}$ are the resonant frequency, upper half power point frequency, lower half power point frequency, passband width, and current values at f_r, f_{c2}, and f_{c1} of traditional RLC [30]. f_{rb},f_{cb1},f_{cb2},BW_b,I_2, $I_{2f_{cb2}}$, $I_{2f_{cb1}}$, and x are the resonant frequencies, the upper passband cutoff frequency, and the lower passband cutoff frequency, the passband width, the current value at f_{rb}, f_{cb2}, and f_{cb1}, a variable less than 1 of wide-band resonance respectively. The relationship between parameters is shown in Eqs 1 -6.

$$f_{rb} = f_r = 1/(2\pi\sqrt{LC}) \tag{1}$$

$$f_{rb} = \sqrt{f_{cb1} f_{cb2}} \tag{2}$$

$$\mathrm{BW} = f_{c2} - f_{c1} = R/L \tag{3}$$

$$\mathrm{BW_b} = f_{cb2} - f_{cb1} \tag{4}$$

$$I_{1f_{c2}}/I_1 = I_{1f_{c2}}/I_1 = 0.707 \tag{5}$$

$$I_{2f_{cb2}}/I_2 = I_{2f_{cb2}}/I_1 = x\ (x < 1) \tag{6}$$

Ref. [30] pp.135–139 shows the derivation process of the traditional RLC resonance equations, and the derivation of the broadband resonance equations is shown in the appendix-A. It can be seen from Fig. 5(c) that the traditional

RLC resonance mode, or multi-frequency resonance, has a narrow passband and strong frequency selectivity in their application scenario (the loop resistance is very small). In the passband BW near the resonant frequency, the current amplitude is large. Beyond the cut-off frequency on both sides of the pass band, the current amplitude drops rapidly. Therefore, this method is more suitable for heavy transmission current with a certain frequency. the narrow-band resonant mode has strong frequency selectivity, and the current amplitude is heavy in the passband BW near the resonant frequency. Beyond the cut-off frequency on both sides of the pass band, the current amplitude drops rapidly. Therefore, this method is more suitable for heavy transmission current with a certain frequency. On the contrary, the broadband resonant mode is characterized by weak frequency selectivity. In the passband BW near the resonant frequency, the current amplitude attenuation is slow and the passband width is large. Therefore, broadband resonance is more suitable for the depth-focused waveform and the GAFDEM. Furthermore, the narrowband resonance can achieve high current (as shown by the blue curve in Fig. 5(c)) in its application context (the resistance is minimal). Due to the large load resistance of GAFDEM, the current in narrowband resonance can only reach the peak of the red curve in Fig 5(c). The current variation range of broadband resonance is the current amplitude contained in the passband. The difference in current between the two methods is not substantial, and will not significantly impact the detection results. After the arrangement of the transmitter system is completed, the electrodes and wires no longer change, and their parameters are easily measurable. We generally consider R and L as known parameters. Therefore, when the broadband resonant circuit is applied to the depth-focused waveform, the key is to determine the parameters f_{rb} and BW_b. When detecting different areas, it is necessary to rearrange the transmitter system, remeasure the R and L values, and design circuit. The depth-focused waveform in Fig. 3 is taken as an example to introduce the principle of parameter determination.

a) The selection principle of BW_b

After the transmission fundamental frequency is determined, the frequencies of the 7, 8, 9, 10, and 11 harmonics of the depth-focused waveform can be determined. Each harmonic frequency is denoted as f_{h7}, f_{h8}, f_{h9}, f_{h10}, and f_{h11}. In different transmission tasks, the harmonic frequency of the depth-focused waveform is not fixed, and it can be seen from Eq. 3 that the bandwidth of the traditional resonance is determined by the resistance and inductance parameters. It will inevitably appear that the resonant passband width is not enough. if we increase the resistance to expand the bandwidth, which will obviously reduce the efficiency of the system. In order to keep each harmonic frequency in the passband, we do not use the passband concept of traditional RLC resonance, which is characterized by the fact that the current amplitude at the passband boundary is 0.707 times the current amplitude at the resonant point. Instead, we think that the passband of the broadband resonance is not a fixed value, and its width is determined by the harmonic distribution of the depth-focused waveform. We no longer pay attention to the relationship between the current amplitude at the passband boundary and the current amplitude at the resonance point. Let $f_{h11} = f_{cb2}$ and $f_{h7} = f_{cb1}$. BW_b can be obtained from Eq. (4). The relationship between I_2 and $I_{2f_{\mathrm{cb2}}}$ and $I_{2f_{\mathrm{cb1}}}$ is shown in Eq. 6.

It can be seen that BW_b is mainly determined by the inductance of the conductor and the upper and lower limiting frequencies contained in the depth-focused waveform. For the depth-focused waveform with more frequencies, the lowest frequency f_{hlow} and the highest frequency f_{hhigh} are equal to f_{cb1} and f_{cb2}, respectively. Then BW_b can be obtained by the same principle.

b) The selection principle of f_{rb} (C)

After obtaining BW_b, f_{rb} can be obtained from Eq. 2 as Eq.7. Further, the value of C can be found according to Eq. 1 as Eq. 8.

$$f_{rb} = \sqrt{f_{h11} f_{h7}} \tag{7}$$

$$C = 1/(4\pi^2 {f_{rb}}^2 L) \tag{8}$$

It can be seen that C is mainly determined by the upper and lower limit frequencies contained in the conductor inductance and the depth focusing waveform. For the depth-focused waveform with more frequencies, the lowest frequency f_{hlow} and the highest frequency f_{hhigh} are equal to f_{cb1} and f_{cb2}, respectively, and f_{rb} can be obtained according to the same principle, and then C can be obtained.

3.2 Matching parameters design and circuit performance analysis

To make the design process clear, the parameter design is carried out according to the previous actual detection situation. Set the fundamental frequency of the depth-focused waveform at 500 Hz and the harmonic frequencies at 3500 Hz, 4000 Hz, 4500 Hz, 5000 Hz, and 5500 Hz as the target transmission frequency. The supply voltage is 12 V. The length of the transmission wire is 2 km, its inductance is about 2 mH. The grounding electrode resistance is 20 Ω. After the basic parameters are determined, it can be seen that f_{h7}= 3500 Hz, f_{h11}= 5500 Hz, and f_{rb}≈ 4387.48 Hz according to Eq. 7, and then C≈0.6579 μF according to Eq. 8. After the circuit parameters are determined, the performance of the designed circuit is analyzed by the the circuit amplitude-frequency response curve.

The amplitude-frequency characteristic curve of the transfer function can reflect the relationship between the

Table 1 Changes in time-domain waveform amplitude, harmonic magnitudes, active power, and reactive power.

	Time-domain amplitude (A)	Harmonic magnitude in the frequency domain					Active power (W)	Reactive power (var)
		7th (A)	8th (A)	9th (A)	10th (A)	11th (A)		
Conventional circuit	0.707	0.11	0.10	0.09	0.09	0.11	1.00	2.84
Broadband resonance	0.346	0.17	0.25	0.28	0.24	0.25	5.80	1.26
Variation	0.361	0.06	0.15	0.19	0.15	0.14	4.80	-1.58
Multiple of change	2.04	1.54	2.50	3.11	2.66	2.27	5.80	0.44

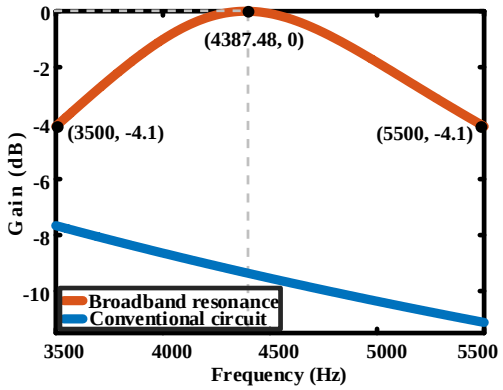

Fig. 6 Comparison of amplitude-frequency response curves between conventional transmitter circuit and broadband resonant circuit

output and input of the circuit at a specific frequency. To display the resonant effect of the designed circuit more intuitively, the transfer function $G(s) = U_1/U_0$ of the circuit is introduced. Where U_1 is the voltage value on R and U_0 is the output voltage of the inverter circuit. According to the voltage-division principle, the transfer function of the conventional transmitter circuit is shown in Eq. 9, and that of the circuit after broadband resonance is added is shown in Eq. 10 [31].

$$\mathrm{G}(s)0 = R/(R + sL) \tag{9}$$

$$\mathrm{G}(s) = \frac{U_1}{U_0} = sR/((\mathrm{s})^2 L + sR + \frac{1}{C}) \tag{10}$$

Fig. 6 shows the amplitude-frequency characteristic curves of the conventional transmitter circuit and the transmitter circuit with broadband resonant in the frequency range of 3500–5500 Hz. The frequency response at the resonant point is 0 dB, and at both sides of the passband is –4.1 dB, which meets the broadband resonance characteristics. At the same time, in the frequency range of 3500–5500 Hz, the frequency domain characteristics are 3.5 dB higher than those of the non-resonant circuit. This means that in the passband of 3500–5500 Hz, under the same input condition, after adding broadband resonance, the circuit output attenuation relative to the input is reduced. A stronger current can be loaded on the transmission wire to improve the intensity of the electromagnetic detection signal.

4. Simulation experiment

4.1 Simulation experiment

To verify the feasibility of the designed circuit, simulation experiment was carried out on the parameters designed in Section 3.2. The frequency domain electromagnetic method

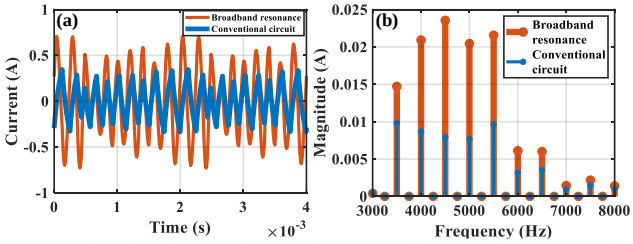

Fig. 7 Time domain waveform and spectrum diagram of conventional transmission and broadband resonant current. (a) Time-domain current waveform. (b) Spectrum.

only pays attention to the current and power at the transmission frequency. Then the active and reactive power of the circuit is analyzed by Eq. 13 and Eq. 14 [32]. In conventional transmitter circuit, $Z_i = Z_{1i}$ is shown as Eq. 11, and in addition to broadband resonance, $Z_i = Z_{2i}$ is shown as Eq. 12.

$$Z_{1i} = R + \mathrm{j}2\pi f_{hi}\mathrm{L} \tag{11}$$

$$Z_{2i} = R + \mathrm{j}2\pi f_{hi}\mathrm{L} - \mathrm{j}/(2\pi f_{hi} c) \tag{12}$$

$$\mathrm{P} = \sum_{i=7}^{11} I_i^2 \, Re(Z_i) \tag{13}$$

$$\mathrm{Q} = \sum_{i=7}^{11} I_i^2 \, Im(Z_i) \tag{14}$$

The simulation results are shown in Fig. 7. Figs. 7(a) and (b), show the current waveform and current spectrum, respectively. In Fig. 7(a), the current waveform of conventional transmitter circuit (blue line) has obvious spikes, and the waveform is similar to a triangular wave. After adding the broadband resonant circuit, the peak of the current waveform (red line) is obviously improved, and the waveform is similar to a sine wave. In the time-domain (a) and frequency-domain (b), the peak amplitude of the red line is higher than that of the blue line. Table 1 shows the changes in time-domain waveform amplitude, each harmonic magnitude, active power, and reactive power in the two circuits.

It can be seen from Table 1 that after broadband resonance was added, the magnitude of the 8th, 9th, 10th, and 11th harmonics increased by more than 2 times, the magnitude of the 7th harmonic increased by about 1.5 times. The maximum lifting times appear at the 9th harmonic, which accords with the character that the maximum current value near the resonant frequency of resonance theory. The active power of the transmitter system was increased by 580 percent, while the reactive power was reduced by 56 percent. Therefore, the current amplitude of multiple frequencies could indeed be increased simultaneously by broadband resonance. Then a stronger current was loaded on the

transmission wire, thus increased the power of the transmitter system. Although it is desirable for the strength of the detection signal to be as high as possible, the broadband resonance method has achieved significant power enhancement without altering the power supply voltage. This improvement is sufficient to meet the detection requirements for medium and short distances.

4.2 Robustness of the broadband resonant method

In field work, the reliability of the method is very important. It has been proved in [23] that the method loses its effectiveness when the capacitance error is 5%. In order to investigate the robustness of the broadband resonant method, we introduce capacitance error to observe the variation of current harmonic magnitude.

The output voltage waveform of the inverter is always constant in the working process. Therefore, the harmonic magnitude of the voltage signal can be calculated according to the energy distribution of the depth-focused waveform described in Section 2. By calculation, when the power supply voltage is 12V, U_7= 5.66 V, U_8= 5.63 V, U_9= 5.70 V, U_{10}= 6.05 V, and U_{11}= 8.30V. The impedance expression of the conventional transmitter circuit (Fig. 2) is shown in Eq. 11, and the current expression is shown in Eq. 15. After broadband resonance is added, the impedance and current of the circuit are calculated as shown in Eq.12 and Eq. 16.

$$|I_{1i}| = |U_i/Z_{1i}| \quad (15)$$

$$|I_{2i}| = |U_i/Z_{2i}| \quad (16)$$

Where |*| represents the module of an imaginary number. The values obtained from Eq. 15 and Eq. 16 are the effective values of each harmonic current.

EACO is the best-quality capacitor that we can buy. Table 2 gives the series of EACO capacitors that can use for resonance and their deviation ranges. Please note that we are analyzing a relatively large range of limit error. In practical applications, capacitors will not exhibit such significant errors. It can be seen that the deviation of the capacitor is generally within the range of ±5% and ±10%. In order to analyze the influence of capacitance error on the resonance effect, the resonance effect of C within the range of deviation ±10% is explored.

According to the calculation results of matching parameters in Section 3.2, the standard values of C is set as 0.6579 μF. With the step sizes of 0.0001 μF, C is 0.5921–0.7237 μF. Each harmonic change is calculated according to Eq.15 and Eq. 16. Fig. 8 shows the current variation with ±10% deviation of capacitor parameters. The solid line is the magnitude change curve of each harmonic magnitude and different colors correspond to different harmonic orders. The dashed line is the theoretical value of each harmonic current in conventional transmitter circuit. The solid line with the same color has the same harmonic frequency as the dashed line.

It can be seen from Fig. 8 that the harmonic magnitude (solid line) in the broadband resonance circuit is higher than

Table 2 Deviation of EACO capacitors.

Version	SRH	SCD	SCH	STD	STC
deviation	±5%,	±5%,	±5%,	±5%,	±5%,
area	±10%	±10%	±10%	±10%	±10%

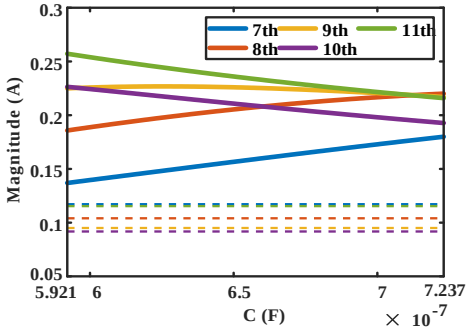

Fig. 8 Variation in harmonic magnitudes within the capacitance error range of ±10%

Table 3 Variation of harmonic magnitudes.

Harmonic	7th	8th	9th	10th	11th
Variation	31%	18%	-3%	-14%	-16%

the harmonic magnitude (dashed line) in the conventional transmitter circuit within the ±10% device deviation range. This indicates that within this deviation range, the broadband resonant circuit is effective. At the same time, it can be seen that the magnitude of the 7th harmonic (blue solid line) is always lower than the magnitude of other harmonics (solid line). This is caused by the uneven energy distribution of the depth-focused waveform and the 7th harmonic with the lowest energy lies at the edge of the passband. Table 3 shows the magnitude variation of each harmonic when the capacitor varies in the range of -10%-+10%. "-" indicates reduction.

Combined with the data of Table 3 and Fig. 8, it can be seen that when C changes within the range of 0.5921-0.7237μF, the magnitudes of harmonics gradually converge. The magnitudes of the 7th and 8th harmonics gradually increase, and the magnitudes of the 9th, 10th, and 11th harmonics gradually decrease. The 7th harmonic increased by 31%, and the 11th harmonic decreased by 16%. The reason is that when the value of C increases, the resonant frequency decreases from 4624 Hz to 4183 Hz. This makes the resonant frequency gradually closer to the 7 and 8 harmonics with lower frequencies and gradually increasing their magnitudes, while deviating from the 9, 10, and 11 harmonics with higher frequencies and gradually decreasing their magnitudes. The above simulation experiments indicate that within a ±10% capacitor error range, the broadband resonance method remains effective. The stability of this method is sufficient to meet the requirements for field work.

5. Experimental verification

To further verify the feasibility of the method, the

Fig. 9 The physical picture of the transmitter circuit.

Table 4 Parameters of experiment.

	Load		Resonant capacitor
	R (Ω)	L (mH)	C (μF)
Standard value	20	2	0.6579
Measured value	19.584	2.0271	0.6429

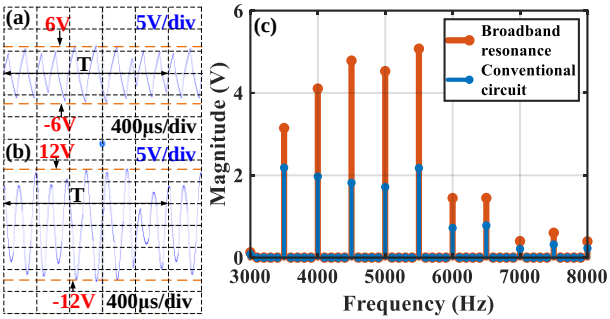

Fig. 10 Experimental result (a) Voltage waveform during conventional transmission. (b) Voltage waveform after adding broadband resonance. (c) Spectrum comparison before and after adding resonance.

transmitter circuit shown in Fig. 9 was built. The transmitter circuit consists of a power supply, load, resonance matching circuit, inverter, and FPGA control circuit. The power supply is a 12 V battery. The standard values and measured values of the devices used are shown in Table 4. The standard values correspond to the parameters mentioned in Section 3.2, while the measured values were measured by the AT826 LCR meter with a measuring accuracy of 0.2%. When the transmitter circuit works, the battery and the FPGA supply power and control signal to the inverter, which outputs the depth-focused voltage waveform to the load (or the load and matching capacitor) to generate transmission current.

Since the voltage at both ends of the resistance is linear with the current, the Tektronix DP03052 oscilloscope was used to observe the voltage of the 19.584 Ω resistance of the load part to characterize the current change of the circuit. Fig. 10, shows the time-domain waveform and spectrum of the resistance voltage before and after adding the resonant matching circuit. Table 5 shows the specific parameter values. It can be observed that after the addition of broadband resonance, the magnitudes of the 7th, 8th, 9th, 10th, and 11th harmonics were increased by 1.44,2.09, 2.64, 2.64 and 2.33 times, the active power was increased by 490%, and the reactive power was decreased by 37%.

Compared with Table 1 and Table 5, the 7–11 harmonics in the simulation experiment were increased by 1.54, 2.50, 3.11, 2.66, and 2.27 times, respectively, the maximum increase occurs at the 9th harmonic. In the experimental results, the 7–11 harmonics are increased by 1.44, 2.09, 2.64, 2.64, and 2.33, respectively, the maximum increase occurred at the 9th and10th harmonic. The reason for this difference is that, on the one hand, the standard resonant frequency of the simulation experiment is 4387 Hz, while it shifts to 4408 Hz due to the error of inductance and capacitance in the experimental prototype, which makes it closer to the 10th harmonic, so the magnitude of the 10th harmonic is further enhanced. On the other hand, the inductance in the experimental prototype is larger than the standard value in the simulation experiment, which makes the magnitude of the 10 harmonics in the conventional transmission inevitably smaller than the standard value. Therefore, it is inevitable that the magnitude of the 10th harmonic will be increased more than that of the simulation experiment. However, by comparing Fig. 7(b), and Fig. 10(c), it can be observed that the harmonic magnitude (red line) of the broadband resonant circuit is larger than that of the conventional transmitter circuit (blue line), and the harmonic magnitude changes in the same way. Both the simulation experiment and the experimental verification can prove that the broadband resonant method can effectively improve the amplitude of the transmission current, enhance the active power, reduce the reactive power, and make the load wire with a heavier current.

6. Conclusion

In GAFDEM, the high-frequency impedance of the load is high. This makes it impossible for the conventional resonant method and the transmission waveform to generate signals with multiple frequencies and large amplitudes in the middle and high-frequency bands. To solve this problem, a broadband resonant circuit structure is designed for the depth-focused waveform of the GAFDEM. The performance of the designed circuit is analyzed by theoretical calculation, and its feasibility is verified by the simulation experiment and experimental verification. The results show that the designed circuit can achieve a good resonance effect within ±10% error of the capacitor. With the addition of the designed circuit, the current amplitude, harmonic magnitudes, and active power of the transmitter system are significantly enhanced. The broadband resonant circuit in this paper is suitable for the depth-focused waveform of GAFDEM. It improves the transmission

Table 5 Changes in time-domain waveform amplitude, harmonic magnitudes, active power, and reactive power.

	Time-domain	Harmonic magnitude in the frequency domain					Active power	Reactive
	amplitude (V)	7th (V)	8th (V)	9th (V)	10th (V)	11th (V)	(W)	power (var)
Conventional circuit	6.00	2.18	1.96	1.81	1.71	2.17	0.99	2.96
Broadband resonance	12.00	3.14	4.10	4.78	4.52	5.07	4.85	1.89
Multiple of change	2.00	1.44	2.09	2.64	2.64	2.33	4.90	0.63

efficiency and the amplitude of the transmission current. It is the first time for low-power systems of the GAFDEM to realize the relatively large multi-frequency current transmission in the middle and high-frequency bands. Compared with the multi-frequency resonance, this method can reduce the number of devices, complexity, and cost of the instrument, which enhances its portability in fieldwork. At the same time, this method reduces the sensitivity of the device parameters. When the device parameters change within a small range, there will be little influence on the resonance effect, making the transmitter circuit's applicability stronger. The new finding of this paper is that even with a single capacitor, it is possible to increase the magnitude of multiple major harmonics of the depth-focused waveform, and it can achieve good results. This paper provides a new solution for the precision and high-efficiency exploration of shallow targets with the GAFDEM.

Acknowledgments

This work was supported by National Natural Science Foundation of China (42127807, 42174085), the Natural Science Foundation of Jilin Province (20220101169JC), the Graduate Innovation Fund of Jilin University.

References

[1] X. Wu, G. Q. Xue, G. Y. Fang, X. Li, and Y. J. Ji, "The Development and Applications of the Semi-Airborne Electromagnetic System in China," IEEE Access, vol. 7, pp. 104956-104966, 2019.

[2] Q. Y. Di, G. Q. Xue, C. C. Yin, and X. Li, "New methods of controlled-source electromagnetic detection in China," Science China. Earth Sciences, vol. 63, (9), pp. 1268-1277, 2020.

[3] T. Mogi, K. Kusunoki, K. Suzuki, K. Kawasaki, A. Jomori, and Y. Azuma, "Development of CSMT instrument using complex phase detector," *Geophysics*, Expl. Japan, 43 (1990), pp. 164-170(in Japanese).

[4] J. He, "Wide field electromagnetic sounding methods," Journal of Central South University (Science and Technology), vol. 41, (3), pp. 1065-1072, 2010.

[5] J. Lin, L. L. Kang, C. S. Liu, T. Y. Ren, H. G. Zhou, and Y. Yao, et al. (2019), "The frequency-domain airborne electromagnetic method with a grounded electrical source," GEOPHYSICS, 84: E269-E280.

[6] J. T. Tang, Z. Y. Ren, C. Zhou, L. C. Zhang, Y. Yuan, and X. Xiao. "Frequency-domain electromagnetic methods for exploration of the shallow subsurface: A review," Chinese Journal of Geophysics (in Chinese), 2015, 58(8): 2681-2705, doi: 10.6038/cjg20150807

[7] J. Lin, J. Chen, F. Liu, and Y. Zhang, "The Helicopter Time-Domain Electromagnetic Technology Advances in China, " Surv Geophysics, 42, 585–624 (2021). https://doi.org/10.1007/s10712-021-09635-7

[8] C. Nittinger, M. Cherevatova, M. Becken, and DESMEX Working Group, "A novel semi-airborne em system for mineral exploration - first results from combined fluxgate and induction coil data," in Second European Airborne Electromagnetics Conference, Sep 2017, Volume 2017, p.1 – 5, DOI: 10.3997/2214-4609.201702154.

[9] M. Becken, C. Nittinger, M. Smirnova, A. Steuer, T. Martin, H. Petersen, et al, "DESMEX; a novel system development for semi-airborne electromagnetic exploration," Geophysics, vol. 85, (6), pp. E239-E253, 2020.

[10] Y. YANG, J. S. He, F. Ling, and Y. Z. Zhu, "Distributed wide field electromagnetic method based on high-order 2n sequence pseudo random signal," Transactions of Nonferrous Metals Society of China, vol. 32, (5), pp. 1609-1622, 2022.

[11] Y. YANG, J. HE and D. Q. LI, "Energy distribution and effective components analysis of 2 sequence pseudo-random signal," Transactions of Nonferrous Metals Society of China, vol. 31, (7), pp. 2102-2115, 2021.

[12] L. H. Gao, S. B. Yu, H. G. Zhou, C. S. Liu, N. Chen, and Y. Huang, "Depth-Focused Waveform Based on SHEPWM Method for Ground-Airborne Frequency-Domain Electromagnetic Survey," IEEE Journal of Selected Topics in Applied Earth Observations and Remote Sensing, vol. 12, (6), pp. 1981-1990, 2019.

[13] L. H. Gao, Y. K. Liu, N. Chen, H. L. Li, N. N. Zhao, and S. B. Yu, "A Design Method of the Transmitting Waveform of Electromagnetic Sounding Based on Selective Harmonic Elimination," Mathematical Problems in Engineering, vol. 2022, pp. 1-12, 2022.

[14] Q. H. Zhen and Q. Y. Di, "High-frequency high-power CSAMT transmitting technology research," Acta Geophysica Sinica, vol. 60, (11), pp. 4160-4164, 2017.

[15] M. Wang, S. Jin, M. Deng, W. B. Wei, and K. Chen, "Multifunction Electromagnetic Transmitting System for Mineral Exploration," IEEE Transactions on Power Electronics, vol. 33, (10), pp. 8288-8297, 2018.

[16] M. Wang, S. Jin, W. B. Wen, and M. D, "The technique analysis and achievement of the high-power borehole-ground electromagnetic synchronous transmitter system," Acta Geophysica Sinica, vol. 62, (10), pp. 3794-3802, 2019.

[17] H. G. Zhou, Y. Yao, C. S. Liu, et al, J. Lin, L. L. Kang, and G. Li, et al, "Feasibility of signal enhancement with multiple grounded-wire sources for a frequency-domain electromagnetic survey," Geophysical Prospecting, vol. 66, (4), pp. 818-832, 2018.

[18] X. J. Wang, Z. H. Fu, Y. Wang, W. D. Wang, W. Liu, and J. L. Zhao, "A wide-frequency constant-amplitude transmitting circuit for frequency domain electromagnetic detection transmitter," Electronics (Basel), vol. 8, (6), pp. 640, 2019.

[19] J. Kim and J. Jeong, "Range-Adaptive Wireless Power Transfer Using Multiloop and Tunable Matching Techniques," IEEE Transactions on Industrial Electronics (1982), vol. 62, (10), pp. 6233-6241, 2015.

[20] Y. Zao, Q. Ouyang, J. W. Chen, X. L. Zhang, and S. C. Hou, "Design and implementation of improved LsCpLp resonant circuit for power supply for high-power electromagnetic acoustic transducer excitation," Review of Scientific Instruments, vol. 88, (8), pp. 084707-084707, 2017.

[21] N. Islam and A. J. Fleming, "Resonance-Enhanced Coupling for Range Extension of Electromagnetic Tracking Systems," in IEEE Transactions on Magnetics, vol. 54, no. 4, pp. 1-9, April 2018, Art no. 5700109, doi: 10.1109/TMAG.2017.2784384.

[22] C. S. Liu, C. F. Zhang, H. G. Zhou, N.J. Liu, and G. Li, "Design of Shallow Surface Electromagnetic Detection Transmitting Scheme Based on Three-Frequency Resonance," IEEE Transactions on Instrumentation and Measurement, vol. 70, pp. 1-9, 2021.

[23] C. S. Liu, S. X. Liu, T. C. Tian, N. J. Liu, and H. G. Zhou, "Realization of Multi-Frequency Resonance for a Portable Near-Surface Frequency-Domain Electromagnetic Transmitting System," IEEE Transactions on Instrumentation and Measurement, vol. 71, pp. 1-10, 2022.

[24] F. Yu and Y. Zhang, "Modeling and control method for high-power electromagnetic transmitter power supplies," Journal of Power Electronics, vol. 13, (4), pp. 679-691, 2013.

[25] M. Wang, M. Deng, Z. L. Wu, X. H. Luo, J. E. Jing, and K. Chen, "New type deployed marine controlled source electromagnetic transmitter system and its experiment application," Acta Geophysica Sinica, vol. 60, (11), pp. 4253-4261, 2017.

[26] C. S. Liu, W. J. Zhu, J. F. Ma, H. G. Zhou, and L. L. Kang, "Analysis of detection range and depth of ground-airborne frequency domain electromagnetic method," Journal of China University of Mining & Technology, vol. 49, (5), pp. 1006-1012, 2020.

[27] Q. Y. Di, G. Q. Xue, Z. X. Wang, Z. G. An, C. M. Fu, R. Wang, D. Lei,

and O. Fayemi, "Development of the emerging electromagnetic methods for deep earth exploration," Acta Geologica Sinica (Beijing), vol. 93, (S1), pp. 313-317, 2019.

[28] Y. J. Ji, Y. Wang, F. D. Zhou, S. Y. Li, Y. P. Zhao, and J. Lin, "Development and application of the grounded long wire source airborne electromagnetic exploration system based on an unmanned airship," Acta Geophysica Sinica, vol. 56, (11), pp. 3640-3650, 2013.

[29] H. G. Zhou, J. Lin, C. S. Liu, L. L. Kang, G. Li, and X. S. Zeng, "Interaction between two adjacent grounded sources in frequency domain semi-airborne electromagnetic survey," Review of Scientific Instruments, vol. 87, (3), pp. 034503-034503, 2016.

[30] H. S. Li, Fundamentals of Circuit Analysis 4th Ed. Beijing: Higher Education Press, 2006, pp.136-139.

[31] K. Ogata, Modern Control Engineering: 5th ed. Beijing: Publishing House of Electronics Industry, 2011, pp398-401.

[32] A. S. Smirnov, N. N. Solonina and K. V. Suslov, "Separate measurement of fundamental and high harmonic energy at consumer inlet - a way to enhancement of electricity use efficiency," in 2010 International Conference on Power System Technology, Zhejiang, China, 2010, pp. 1-5, doi: 10.1109/POWERCON.2010.5666617.

Shengbao Yu received the B.S. degree from the Dalian University of Technology, Dalian, China, in 1985, and the M.S. and Ph.D. degrees from Jilin University, Changchun, China, in 2000 and 2007, respectively.

He is currently a Professor and a Ph.D. Supervisor with Jilin University. His research interests include geo-exploration and instrumentation.

Fanze Meng received the B.S. degree from the college of Instrumentation and Electrical Engineering, Jilin University, Changchun, China, in 2021, where she is currently pursuing the M.S. degree.

His research interests include ground-airborne frequency-domain electromagnetic instruments and their applications.

Yihan Shen received the B.S. degree from the college of Instrumentation and Electrical Engineering, Jilin University, Changchun, China, in 2020, where she is currently pursuing the Ph.D. degree.

Her current research interest is Electromagnetic exploration, especially transient electromagnetic method.

Yuzhu Hao received the B.S. degree from the college of Instrumentation and Electrical Engineering, Jilin University, Changchun, China, in 2020, where she is currently pursuing the MA.Eng degree.

Her current research interest is Electromagnetic exploration, especially frequency electromagnetic method.

Haigen Zhou received the B.S. degree in electrical engineering and automation and the Ph.D. degree in measurement technology and instruments from Jilin University, Changchun, China, in 2012 and 2017, respectively.

He is currently a Lecturer with Jilin University. His research interests include ground-airborne frequency-domain electromagnetic instruments and their applications.

Appendix – A Derivation of broadband resonance.

According to the circuit in Fig. 4b, the total impedance of the circuit is Eq. 12.

The presence of frequency f_{rb} makes Eq. A · 1 valid.

$$2\pi f_{rb}\mathrm{L} = 1/(2\pi f_{rb}C) \qquad (\mathrm{A}\cdot 1)$$

The imaginary part of the circuit impedance Z is 0, that is, it has Eq. A · 2 at frequency f_{rb}

$$\mathrm{Z}(f_{rb}) = R \qquad (\mathrm{A}\cdot 2)$$

The frequency f_{rb} is called the resonant frequency

According to the definition of broadband resonance, we have Eq. A · 3

$$I_f/I_{f_r} = x \qquad (\mathrm{A}\cdot 3)$$

We know

$$I_{frb} = U_s/R \qquad (\mathrm{A}\cdot 4)$$

Other frequency currents are

$$I_f = U_s/\sqrt{(R)^2 + (2\pi fL - 1/2\pi fC)^2} \qquad (\mathrm{A}\cdot 5)$$

We put A · 4, A · 5 into A · 3

$$2\pi fL - 1/2\pi fC = \pm\sqrt{(1-x^2)/x^2}R \qquad (\mathrm{A}\cdot 6)$$

Then

$$f = \pm\frac{\sqrt{(1-x^2)/x^2}R}{4\pi L} \pm \frac{\sqrt{(1-x^2)/x^2R^2 + 4L/C}}{4\pi L} \qquad (\mathrm{A}\cdot 7)$$

Since f is positive, there are upper and lower passband cutoff frequencies f_{cb2} and f_{cb1}.

$$f_{cb2} = \frac{\sqrt{(1-x^2)/x^2}R}{4\pi L} + \frac{\sqrt{(1-x^2)/x^2R^2 + 4L/C}}{4\pi L} \qquad (\mathrm{A}\cdot 8)$$

$$f_{cb1} = -\frac{\sqrt{(1-x^2)/x^2}R}{4\pi L} + \frac{\sqrt{(1-x^2)/x^2R^2 + 4L/C}}{4\pi L} \qquad (\mathrm{A}\cdot 9)$$

Multiply the Eqs. A · 8 and A · 9 we get

$$f_{cb1}f_{cb2} = 1/4\pi^2 LC \qquad (\mathrm{A}\cdot 10)$$

Substituting Eq. 1 into Eq. A · 10 gives Eq. A · 11

$$f_{cb1}f_{cb2} = f_{rb}^2 \qquad (\mathrm{A}\cdot 11)$$

Then we have Eq. A · 12, which is the Eq. 2.

$$f_{rb} = \sqrt{f_{cb1}f_{cb2}} \qquad (\mathrm{A}\cdot 12)$$